

# Mycolactone-mediated neurite degeneration and functional effects in cultured human and rat DRG neurons: Mechanisms underlying hypoalgesia in Buruli ulcer

U Anand, BSc, MSc, PhD<sup>1</sup>, M Sinisi, MD<sup>2</sup>, M Fox, MBBS, BSc, FRCS<sup>2</sup>, A MacQuillan, MBBS, MRCS(G), MD, FRCS<sup>2</sup>, T Quick, MA, FRCS<sup>2</sup>, Y Korchev, PhD<sup>1</sup>, C Bountra, PhD<sup>3</sup>, T McCarthy, PhD<sup>4</sup> and P Anand, MD, MRCP, FRCP<sup>1</sup>

## Abstract

**Background:** Mycolactone is a polyketide toxin secreted by the mycobacterium *Mycobacterium ulcerans*, responsible for the extensive hypoalgesic skin lesions characteristic of patients with Buruli ulcer. A recent pre-clinical study proposed that mycolactone may produce analgesia via activation of the angiotensin II type 2 receptor (AT<sub>2</sub>R). In contrast, AT<sub>2</sub>R antagonist EMA401 has shown analgesic efficacy in animal models and clinical trials for neuropathic pain. We therefore investigated the morphological and functional effects of mycolactone in cultured human and rat dorsal root ganglia (DRG) neurons and the role of AT<sub>2</sub>R using EMA401. Primary sensory neurons were prepared from avulsed cervical human DRG and rat DRG; 24 h after plating, neurons were incubated for 24 to 96 h with synthetic mycolactone A/B, followed by immunostaining with antibodies to PGP9.5, Gap43,  $\beta$  tubulin, or Mitotracker dye staining. Acute functional effects were examined by measuring capsaicin responses with calcium imaging in DRG neuronal cultures treated with mycolactone.

**Results:** *Morphological effects:* Mycolactone-treated cultures showed dramatically reduced numbers of surviving neurons and non-neuronal cells, reduced Gap43 and  $\beta$  tubulin expression, degenerating neurites and reduced cell body diameter, compared with controls. Dose-related reduction of neurite length was observed in mycolactone-treated cultures. Mitochondria were distributed throughout the length of neurites and soma of control neurons, but clustered in the neurites and soma of mycolactone-treated neurons. *Functional effects:* Mycolactone-treated human and rat DRG neurons showed dose-related inhibition of capsaicin responses, which were reversed by calcineurin inhibitor cyclosporine and phosphodiesterase inhibitor 3-isobutyl-1-Methylxanthine, indicating involvement of cAMP/ATP reduction. The morphological and functional effects of mycolactone were not altered by Angiotensin II or AT<sub>2</sub>R antagonist EMA401.

**Conclusion:** Mycolactone induces toxic effects in DRG neurons, leading to impaired nociceptor function, neurite degeneration, and cell death, resembling the cutaneous hypoalgesia and nerve damage in individuals with *M. Ulcerans* infection.

## Keywords

Buruli ulcer, hypoalgesia, calcium influx, neurite degeneration, apoptosis, TRPV1, mitochondria, mycolactone, neurons

Date received: 3 March 2016; revised: 27 April 2016; accepted: 16 May 2016

<sup>1</sup>Department of Medicine, Imperial College London, Hammersmith Hospital, London, UK

<sup>2</sup>Peripheral Nerve Injury Unit, Royal National Orthopaedic Hospital, Middlesex, UK

<sup>3</sup>University of Oxford Structural Genomics Consortium, Headington, Oxford, UK

<sup>4</sup>Spinifex Pharmaceuticals Pty Ltd, St. Preston, VIC, Australia

### Corresponding author:

U Anand, Department of Medicine, Imperial College London, Hammersmith Hospital, London W12 0NN, UK.

Email: u.anand@imperial.ac.uk



## Background

Buruli ulcer is an infectious necrotizing skin disease caused by Mycolactone (ML), a lipid macrolide toxin secreted by the causative bacteria *Mycobacterium ulcerans*, with the third highest incidence of mycobacterial disease after tuberculosis and leprosy. It is a neglected tropical disease that causes significant disfigurement, affecting mostly malnourished children and fewer adults.<sup>1,2</sup> Infected individuals develop a subcutaneous painless nodule that ulcerates, leading to extensive necrotic skin lesions with loss of adipose and nerve tissue often extending to muscle and bone, resulting in severe deformity. Antibiotic therapy with Rifampicin and Streptomycin is effective, but major reconstructive surgery is often required.<sup>1,3</sup>

The cytotoxic effects of ML are known in a variety of cell types including epithelial cells,<sup>4,5</sup> adipocytes,<sup>6</sup> fibroblasts,<sup>7,8</sup> and monocytes.<sup>9</sup> Cultured fibroblasts and macrophage cell lines treated with ML show cell rounding, inhibition of protein synthesis, and cell-cycle arrest in G0/G1 leading to cell death.<sup>7</sup> However, little information is available regarding the molecular and cellular mechanisms underlying the analgesia that is typical of Buruli ulcer. A direct effect on nerves is indicated from studies of mouse footpad inoculation with *M. ulcerans*, resulting in nerve bundle invasion and damage.<sup>10</sup> Subcutaneous injection with the toxin ML A/B in guinea pigs caused transient hyperaesthesia and cutaneous lesions, with subsequent sensory deficit due to nerve damage.<sup>9,11</sup> A recent report, however, proposed that the analgesic effects of ML in rodents may not involve nerve damage and could be mediated by potassium-dependent hyperpolarization via the angiotensin II (AngII) type 2 receptor (AT<sub>2</sub>R).<sup>12</sup>

A characteristic feature of Buruli ulcer is the absence of an inflammatory response, with T cell depletion in peripheral lymph nodes and lack of a lymphocyte homing response, involving depleted synthesis of cytokines and inflammatory mediators,<sup>13,14</sup> features that are mimicked *in vitro* by ML. A molecular mechanism of aberrant translocation of secreted cytokine proteins has also been proposed to underlie the pathogenic effect of ML<sup>15</sup> and lack of inflammatory hyperalgesia.

The slow growth of *M. Ulcerans*, and limited availability of its secreted toxin ML, which is comprised of two macrolides A and B,<sup>7</sup> led to the chemical synthesis of ML A/B, providing a chemically well-defined molecule facilitating further studies, and which has been used in this study.<sup>16</sup> To investigate the mechanisms of ML-induced analgesia, we examined the morphological effects of synthetic ML A/B on neurites and mitochondrial distribution in cultured human and rat dorsal root ganglion neurons. As nociceptive DRG neurons are activated by a number of noxious agents including capsaicin (the hot ingredient of chilli peppers),<sup>17</sup> we also determined the functional effects of ML on transient receptor potential vanilloid subtype 1 (TRPV1) activation<sup>18</sup> by measuring

calcium influx in response to capsaicin. The potential role of AT<sub>2</sub>R was investigated by using its endogenous ligand AngII and selective antagonist EMA401, using previously described techniques.<sup>19</sup>

## Methods

### Preparation of Human DRG neurons

Cultured neurons were prepared as previously described,<sup>19</sup> briefly, avulsed human cervical DRG (hDRG) were obtained as a necessary part of the surgical nerve repair procedure from three patients, with full informed consent and approval of the Local Research Ethics Committee, Royal National Orthopaedic Hospital, Stanmore, UK. Tissue was enzyme-digested and mechanically dissociated to yield a neuronal suspension, which was plated on collagen and laminin-coated glass bottomed MatTek dishes (MatTek Corp., Ashland, MA, USA) in Ham's F12 medium containing 10% heat-inactivated fetal calf serum, penicillin and streptomycin (100 mg/mL each), the neurotrophic factors (NTFs), nerve growth factor (100 ng/mL), and glial cell-line derived NTF (50 ng/mL). Cultures were incubated at 37°C in a humid environment containing 5% CO<sub>2</sub>/air for 48 h before calcium imaging studies.

### Preparation of rat (rDRG) neurons

Bilateral DRG from all levels were harvested from 10 adult female Wistar rats (Charles River UK Ltd, Margate, Kent, UK) and neuronal cultures were prepared as previously described,<sup>19</sup> and incubated in BSF2 medium (containing 2% heat inactivated fetal calf serum, 0.1 mg/mL transferrin, 60 ng/mL progesterone, 0.16 mg/mL sodium selenite, 3 mg/mL bovine serum albumen (BSA), penicillin/streptomycin 100 mg/mL each, 16 mg/mL putrescine, 10 mg/mL insulin) and NTFs for 24 h. Calcium imaging studies were conducted 48 h after plating.

### Morphological effects

Twenty-four hours after plating, rDRG cultures were treated with 1, 10, or 100 nmol/L ML for 24–96 h and compared with vehicle-treated controls (0.2% ethanol) in duplicate, followed by 4% paraformaldehyde fixation for 20 min. ML doses selected were in the range of previous studies, for epithelial cells 0.1–100 ng/ml, (0.135–135 nmol/L),<sup>4,5</sup> and monocytes 300 pg/ml, (400 nmol/L).<sup>9</sup> For immunostaining and morphological assessments, neurons were permeabilized with methanol (–20°C, 3 min), washed with PBS, immunostained with primary antibodies to Gap43 (mouse monoclonal, 1:200; Sigma), or mouse monoclonal anti  $\beta$ -tubulin III (T8578 Sigma, 1:200), or rabbit anti PGP9.5 (1:500, Ultraclone, UK), and visualized with donkey anti-mouse IgG (Alexa 488,

1:200; Molecular Probes), goat anti-mouse IgG (Alexa 488, 1:200; Molecular Probes), or goat anti-rabbit IgG (Alexa 488, 1:200; Molecular Probes), for 1 h each at room temperature. The glass bottom cover slips were mounted on glass slides in glycerol containing Hoechst dye 33342 and anti-fade agent DABCO [1,4-diazobicyclo-(2,2,2)-octane], and sealed with nail varnish. Tiff fluorescence images were acquired with an upright Olympus microscope (BX43, Olympus Medical, Essex, UK) using Cellsens software (Olympus, Japan) and widefield epifluorescence optics, after confirming the absence of immunostaining in negative controls, where the primary antibody had been omitted. The longest neurite length was measured from individually identifiable neurons in the ML-treated and vehicle-treated groups of cultures, using Cellsens software (Olympus, Japan), and the average is expressed as percent of control.

### *Live cell confocal imaging of mitochondria*

Forty-eight hours after plating, neuronal cultures were treated with 100 nmol/L ML or vehicle for 48 h, then rinsed in HEPES buffered Hanks balanced salt solution (HBSS) containing 0.1% BSA, and incubated in this solution with 50 nmol/L Mitotracker Green FM dye (M-7514, Life Technologies) for 30 min at 37°C. The dye was washed off and the cells were imaged in HEPES buffered HBSS on a Leica TCS SP5 II confocal microscope, using fluoresceine isothiocyanate and DAPI settings for TIFF image acquisition. A separate group of neuronal cultures were similarly treated with 100 nmol/L ML or vehicle for 48 h, and labeled with Mitotracker Red as described above, followed by 4% paraformaldehyde fixation for 15 min. Cultures were then permeabilised with methanol and immunostained with mouse monoclonal anti  $\beta$ -tubulin III (T8578 Sigma, 1:200), visualized with fluoresceine isothiocyanate conjugated goat anti mouse secondary antibody (1:200, Sigma). Coverslips were mounted as described above, and confocal images were acquired.

### *Calcium imaging*

Functional effects of acute ML treatment were assessed by measuring capsaicin responses via TRPV1 in 2  $\mu$ mol/L Fura2 AM (Molecular Probes Life Technologies, Paisley, UK) loaded neurons, as previously described.<sup>19</sup> Responses to paired capsaicin stimuli, with and without ML, EMA401, or AngII were measured as a change in the baseline 340/380  $\lambda_{ex}$  nm ratio before, during, and after addition. Experiments were conducted at 37°C in a humidified environment on an inverted Nikon microscope (Diaphot 300; Nikon, UK Ltd, Kingston upon Thames, Surrey, UK), using alternate excitation at 340 and 380 nm  $\lambda_{ex}$ /510  $\lambda_{em}$  wavelengths; images were acquired every 2 s.

Lyophilized AngII was reconstituted in sterile distilled water, aliquoted, and stored at  $-20^{\circ}\text{C}$ . EMA401 was dissolved in HBSS containing 0.1% BSA (pH 7.4) and stored at 4°C. Synthetic ML A/B, 0.2 mg/ml in DMSO was kindly provided by Prof. Y. Kishi (Harvard University, USA), aliquoted, and stored at  $-20^{\circ}\text{C}$ ; fresh aliquots were thawed immediately before use, and further diluted in ethanol to 500  $\times$  final concentration. All chemicals were obtained from Sigma, Poole, UK, unless stated otherwise. Student's unpaired *t*-Test was used to compare between groups; \* $p < 0.05$  was considered to be statistically significant.

## **Results**

### *Effect of ML on neurites*

Morphological effects of ML in rDRG neurons were apparent 24 h after treatment, when PGP9.5 immunostaining showed fewer surviving neurons with smaller, degenerating neurites, compared with controls (Figure 1(a)–(f)). ML-treated cultures showed a dramatic loss of neurons and non-neuronal cells with surviving cells appearing shrunken at higher doses, having reduced cytoplasm and compact, very bright nuclei, and indicative of apoptosis. The neurite outgrowth assay showed a dose dependent decrease in neurite length after 24 h ML treatment, compared to controls (Figure 1(g)). The average maximum neurite lengths were decreased with ML treatment, and statistically significant at 100 nmol/L ML (\* $p < 0.05$ , paired *t*-Test);  $n = 3$  experiments, total 318 neurons. Neurite loss was greater after 48 h 100 nmol/L ML treatment (\*\* $p = 0.010$ ), and was not affected by the presence of 100 nmol/L EMA401 (\*\* $p = 0.007$ ) (Figure 1(h));  $n = 3$  experiments, total 302 neurons.

### *Effect of ML on Gap43*

Gap43 immunostaining was uniformly distributed in the cell bodies and neurites of control neurons (Figure 2(a), (b)) but was very bright in the surviving neuronal cell bodies and very faint in the degenerating neurites, in neurons treated with ML for 96 h (Figure 2(c), (d)), indicating accumulation in the cell body and reduced axonal transport. Similarly, non-neuronal cells, predominantly Schwann cells and fibroblasts, showed prominent nuclei surrounded by substantial cytoplasm (Figure 2(e)). ML-treated cultures had shrunken cells with little or no cytoplasm and small very bright nuclei (Figure 2(f)).

### *Effect of ML on mitochondria and $\beta$ tubulin*

Confocal imaging showed uniformly distributed  $\beta$  tubulin in the soma and neurites of control neurons colocalized with evenly dispersed Mitotracker red-stained

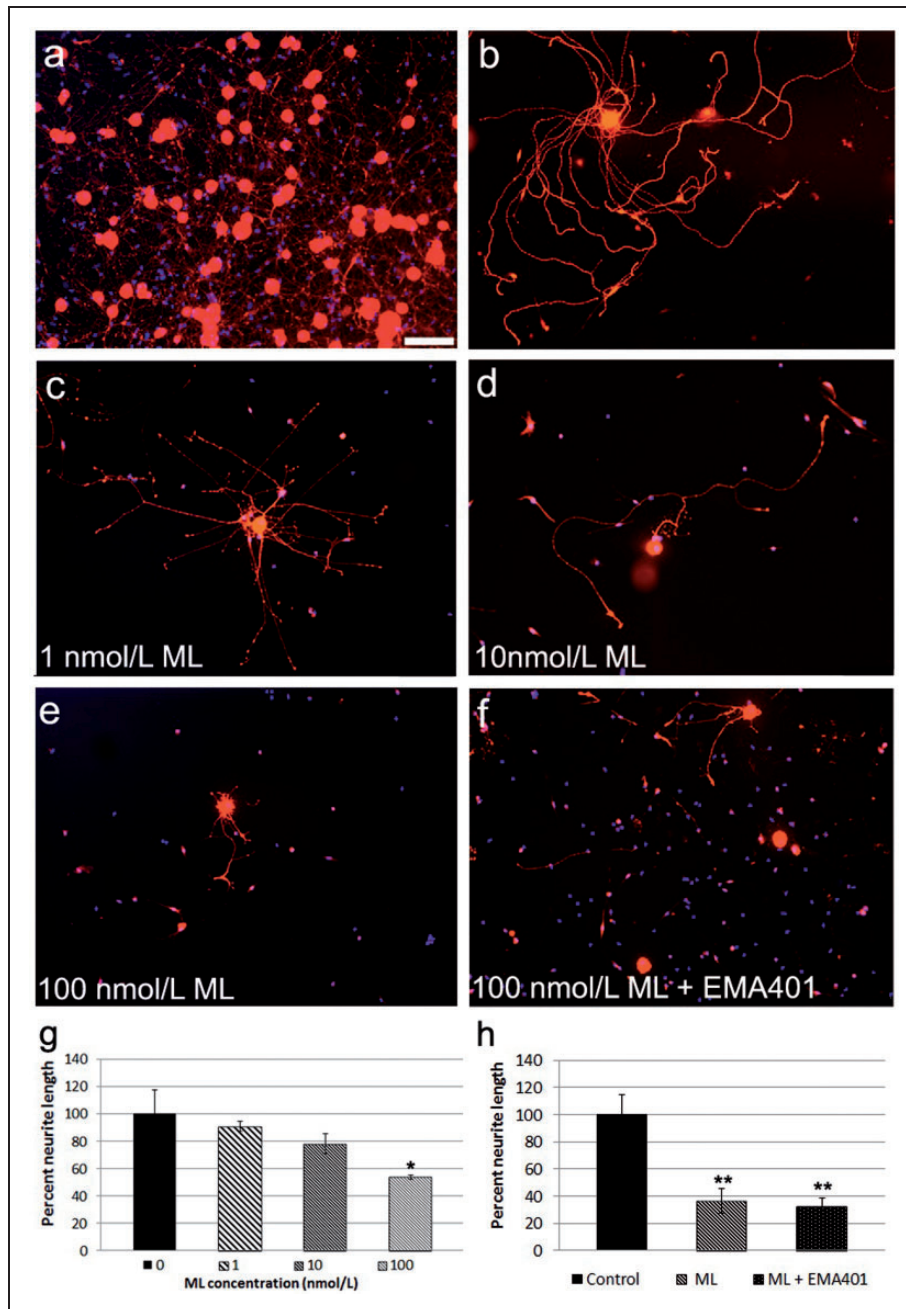


**Figure 1.** Loss of neurites in ML-treated rDRG neurons. PGP9.5 immunofluorescent neurons in control DRG cultures showing dense clusters (a) and a single neuron with profuse neurite outgrowth (b); Dose-related loss of neurites was observed after 24 h treatment with 1 nmol/L ML (c); 10 nmol/L ML (d); and 100 nmol/L ML (e); Co-incubation with the AT<sub>2</sub>R antagonist EMA401 did not affect ML-induced neurite degeneration (100 nmol/L each) (f); Graphs showing summary of neurite lengths after 24 h ML treatment (\**p* < 0.05, paired *t*-test) (g); Neurite lengths were significantly reduced after 48-h treatment with 100 nmol/L ML (\*\**p* = 0.010), and similar to neurons treated with combined EMA401 and ML (100 nmol/L each, \*\**p* = 0.007) (h). Bar in (a) = 50 μm (same magnification in b–h).

mitochondria (Figure 3(a)–(d)). ML-treated neurons showed greatly reduced β tubulin in the soma and complete loss of staining in the neurites, with clumped mitochondria concentrated in the cell bodies and neurites of ML-treated neurons and brightly stained nuclei (Figure 3(e)–(h)). This was confirmed with live cell

confocal imaging using the Mitotracker Green FM dye, which also showed uniformly dispersed mitochondria along the entire length of neurites and cell body in control neurons (Figure 3(i), (j)), while ML treatment resulted in clumped mitochondria that were accumulated in the cell bodies (Figure 3(k)).

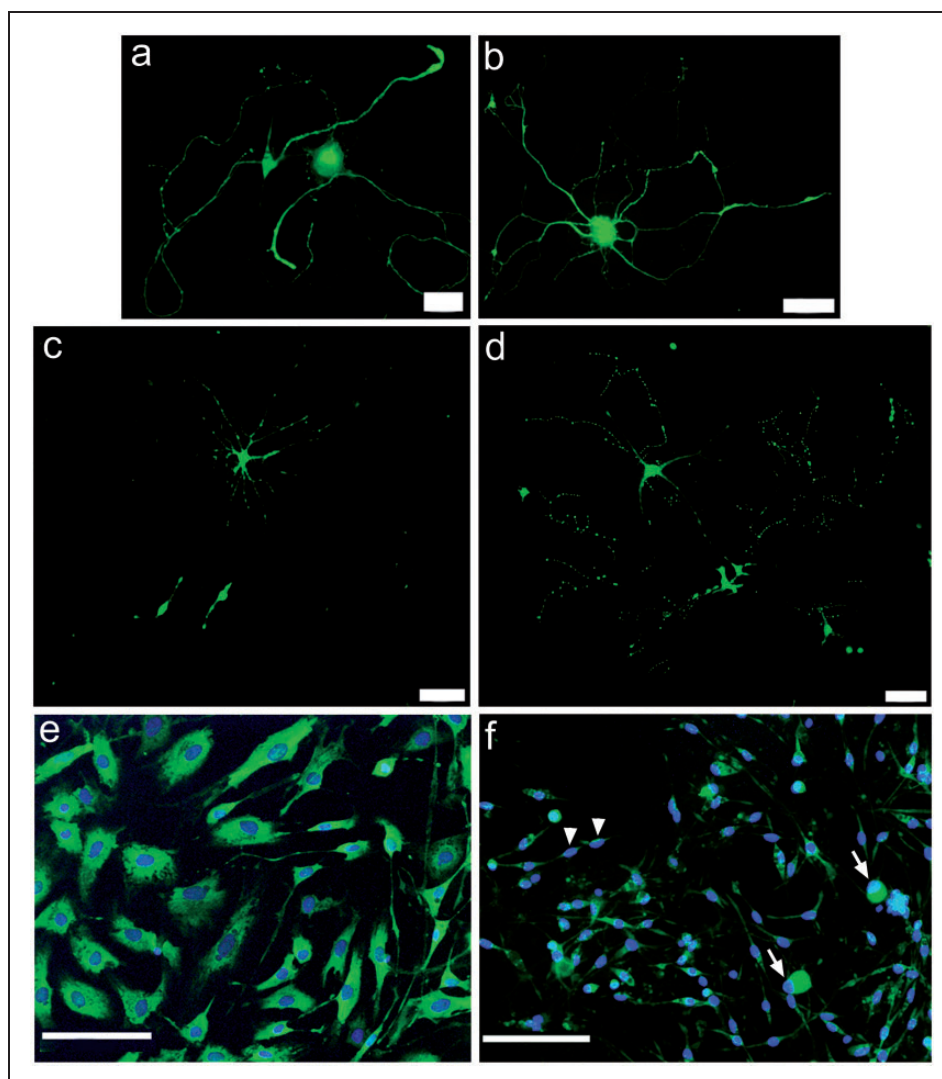


**Figure 2.** Gap43 immunofluorescence was localized in the cell bodies and long profuse neurites in individual control rDRG neurons (a, b). Surviving neurons after 100 nmol/L ML treatment for 96 h showed shrunken cell bodies with disintegrated neurites (c, d). Non-neuronal cells comprising Schwann cells and fibroblasts in control cultures showed well-spread viable cells with distinct cytoplasm and nuclei (e). ML treatment resulted in shrunken neurons (arrows) and non-neuronal cells (arrowheads), with bright condensed nuclei typical of apoptosis (f). Bar in (a) and (c) = 20  $\mu$ m, in (b) and (d) = 50  $\mu$ m, and in (e) and (f) = 100  $\mu$ m.

### Effect of ML on capsaicin responses in human DRG cultured neurons

Acute functional effects of ML were apparent in rDRG and hDRG neurons, 10 min after application, as dose-related inhibition of capsaicin responses. In hDRG neurons, incubation with high dose ML (1.3  $\mu$ mol/L) completely inhibited capsaicin responses, but was reversed following a 30-min rest period after washout (Figure 4(a)–(d)). Dose-related inhibition of capsaicin responses was observed (Figure 4(e)). Percent inhibition  $\pm$  s.e.m. with 260 nmol/L (equivalent to 200 ng/ml) ML was  $69 \pm 12\%$ ,  $n = 7$  neurons,  $**p = 0.003$ ; and with 1.3  $\mu$ mol/L (1  $\mu$ g/ml) ML was  $98.3 \pm 0.7\%$ ,  $n = 3$  neurons,  $**p = 0.004$ . Tachyphylaxis to repeat capsaicin

challenge alone, as control, was similar to previous studies,  $19.3 \pm 5.5\%$  (eight neurons).

### Effect of ML on capsaicin responses in rDRG-cultured neurons

In rDRG neurons, capsaicin responses were blocked in the presence of 300 nmol/L ML (Figure 5(a), (b)); this effect was reversible following a 30-min rest period after washout, when capsaicin sensitivity was restored (Figure 5(c)). Dose-related inhibition of capsaicin responses was observed in the presence of ML (Figure 5(d));  $n = 3$  experiments, (% inhibition  $\pm$  s.e.m): 0 nmol/L ML,  $18.9 \pm 4.4$ , 28 neurons), 3 nmol/L ML, ( $48.1 \pm 7.2$ , 8 neurons), 10 nmol/L ML, ( $62.1 \pm 6.6$ ,

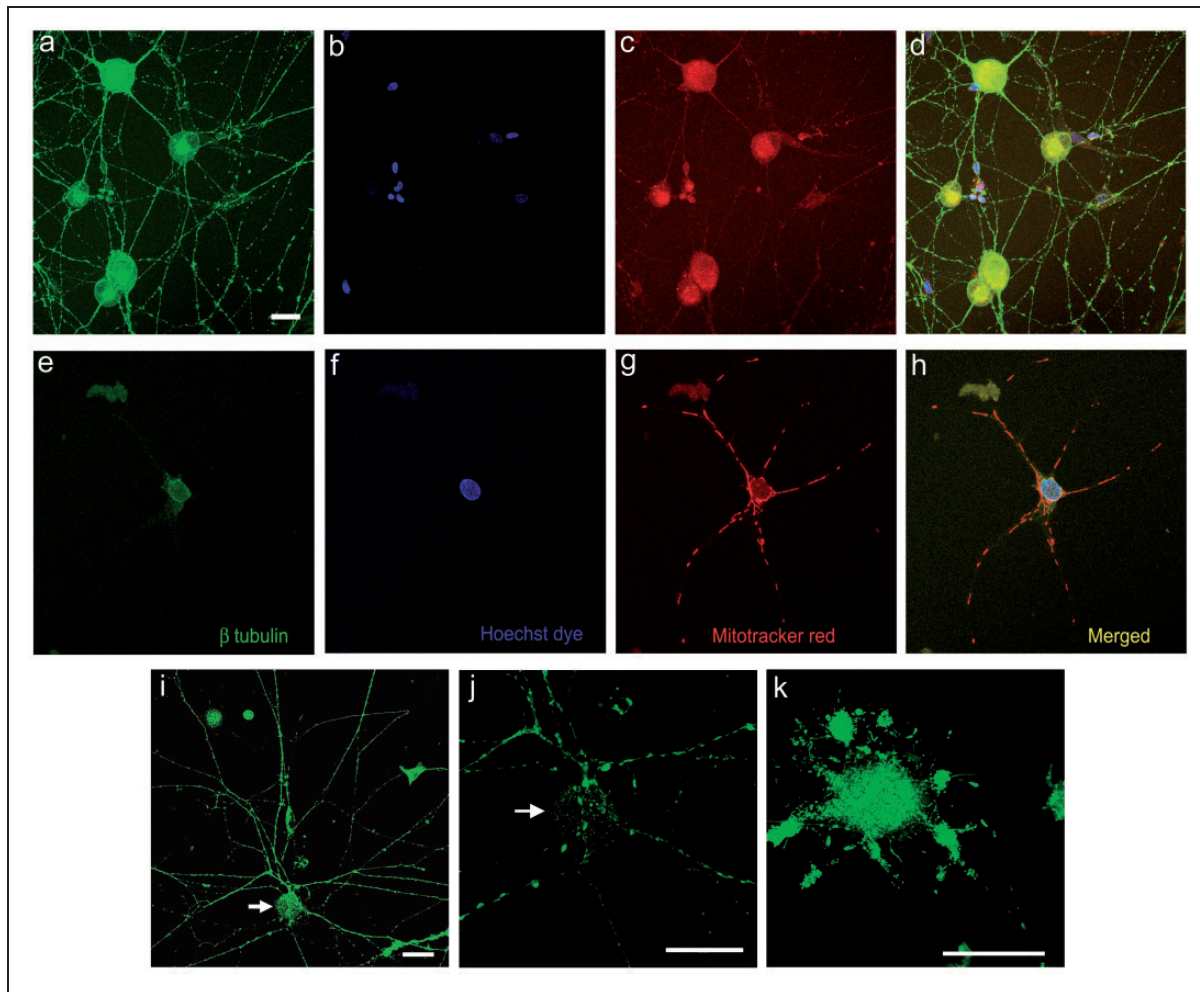


**Figure 3.** ML effect on rDRG neurons. Low power confocal images of control neurons (a–d) showing uniform distribution of  $\beta$  tubulin in the cell body and neurites (a), Hoechst dye stained nuclei (b), uniformly dispersed Mitotracker red labeled mitochondria (c) and the merged image with overlapping  $\beta$  tubulin and mitochondria (yellow, d). ML-treated neuron (100 nmol/L for 48 h) (e–h), showing loss of neurites and  $\beta$  tubulin (e), prominent nucleus (f), clumped Mitotracker Red positive mitochondria (g), and merged image (h). Live cell Mitotracker green labeling of mitochondria which are dispersed throughout the cell body (arrow) and neurites in a control neuron (i), and high power confocal images of the same neuron (j). In a ML-treated neuron, the Mitotracker label shows clumping of mitochondria restricted to the cell body, and loss of neurites (k). Bar in (a) = 25 microns (a–h same magnification).

14 neurons), 30 nmol/L ML, ( $69.6 \pm 4.9$ , 20 neurons), 100 nmol/L ML, ( $85.6 \pm 5.1$ , 26 neurons), 300 nmol/L ML, ( $96.2 \pm 1.1$ , 21 neurons),  $IC_{50} = 10$  nmol/L. The inhibition of capsaicin response by 300 nmol/L ML was not affected by 100 nM AngII ( $96.9 \pm 1.4$ , 7 neurons,  $p > 0.05$ ). Similarly, capsaicin inhibition by 10 nmol/L ML was not affected by the presence of 100 nmol/L EMA401 ( $68.8 \pm 10.4$ , 5 neurons,  $p > 0.05$ ). Application of 100 nmol/L or 1  $\mu$ mol/L ML alone did not stimulate calcium influx (data not shown). Inhibition of capsaicin response by 100 nmol/L ML ( $85.6 \pm 5.1$ , 26 neurons) was abolished in the presence of 10  $\mu$ mol/L cyclosporine (calcineurin inhibitor,  $25.3 \pm 3$ , 21 neurons), and 66  $\mu$ mol/L IBMX (3-isobutyl-1-Methylxanthine; phosphodiesterase inhibitor,  $15.5 \pm 3.9$ , 27 neurons) (Figure 5(e)).

## Discussion

This study shows that ML treatment of DRG cell cultures had extensive morphological and functional effects, targeting both neurons and non-neuronal cells. These effects were seen across all neuronal cell sizes, indicating the absence of a selective effect on any particular sub-population. We observed neurite degeneration and cell death, reduced Gap43 and loss of  $\beta$  tubulin, mitochondrial clumping, and TRPV1 inhibition in ML-treated DRG neurons. These findings are likely to contribute to the lack of pain in Buruli ulcer infection.

ML secreted by *Mycobacterium ulcerans* is known to cause the extensive skin lesions typical of Buruli ulcer, which despite their severity are hypoalgesic. Previous

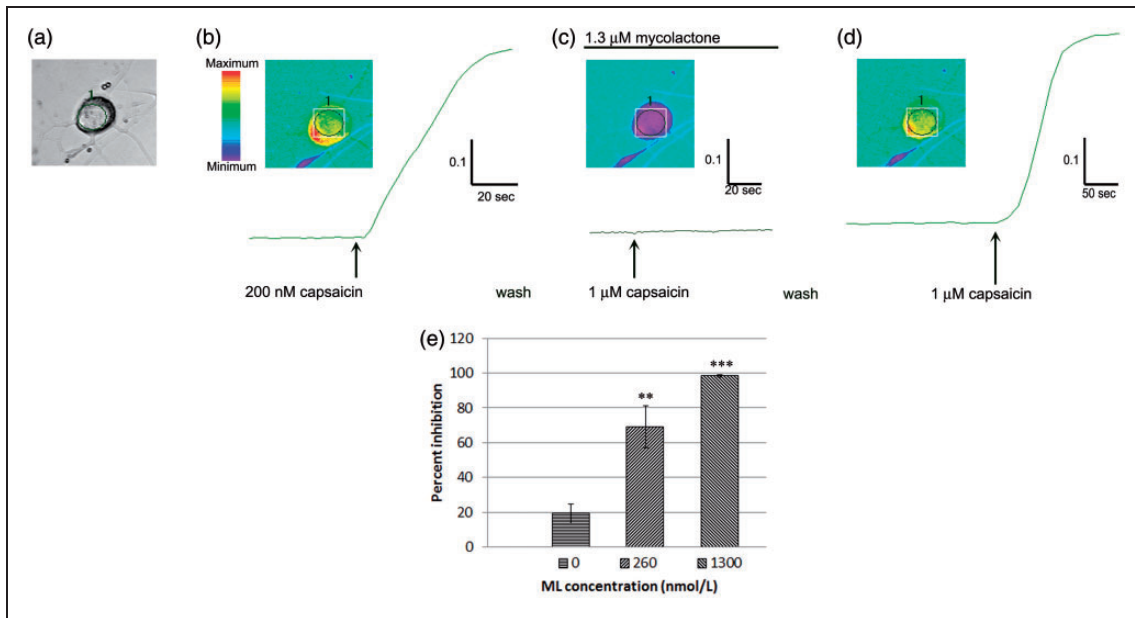


**Figure 4.** Acute effects of ML on capsaicin responses in hDRG neurons. Brightfield image of a human DRG neuron (a), showing increased fura 2 ratio in response to 200 nM capsaicin and the corresponding trace (b), followed by complete inhibition of 1 mol/L capsaicin response in the presence of 1.3 mol/L ML (c). The acute inhibitory effect of ML was reversible following washout, and the capsaicin response was restored (d). Graph showing percent inhibition of responses to 1 M capsaicin dose dependently inhibited in the presence of 260 nmol/L ML (\*\* $p = 0.003$ ) and 1.3 mol/L ML (\*\* $p = 0.004$ ) (e).

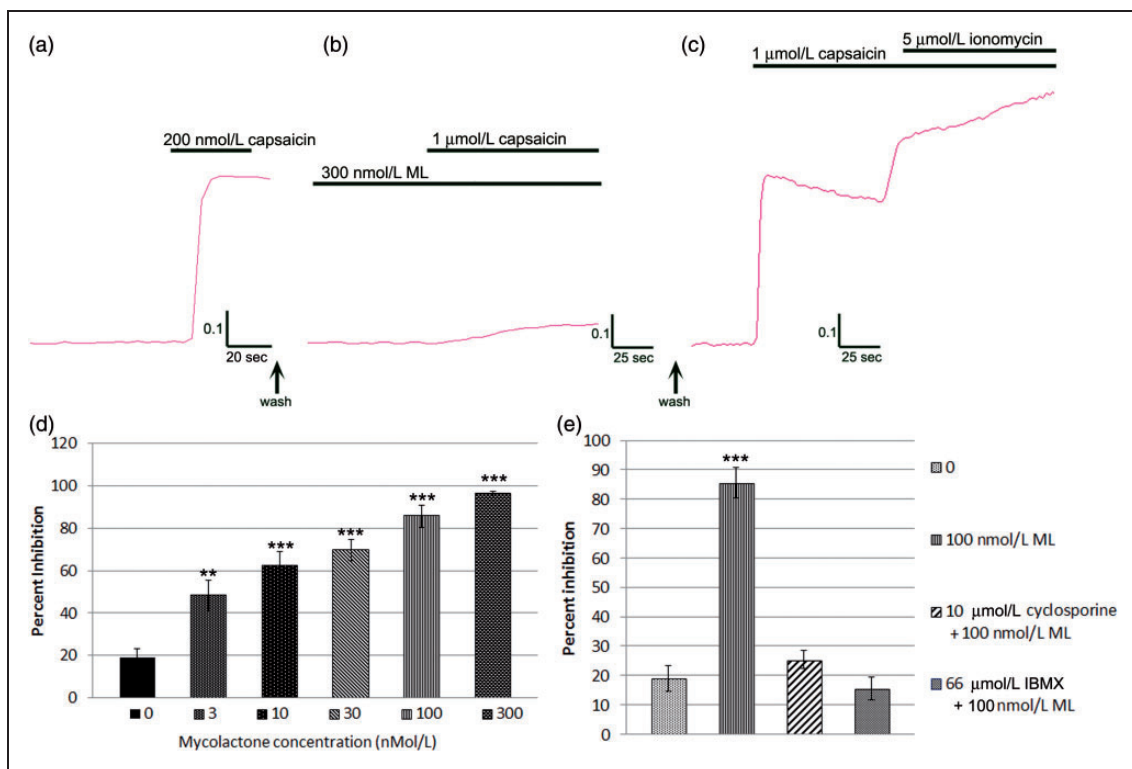


**Figure 5.** Acute effects of ML on capsaicin responses in rDRG neurons. Trace showing increased fura2 ratio in response to 200 nM capsaicin (a). Near complete inhibition was observed in the presence of ML 300 nmol/L (b). The acute inhibitory effect of ML was reversed following a 30-min rest period after washout, and robust responses to capsaicin and ionomycin were observed (c). Graph showing ML dose-related inhibition of capsaicin responses following acute incubation with ML (d). Graph showing inhibition of capsaicin responses by 100 nmol/L ML, which were abolished in the presence of cyclosporine and IBMX (e). \* $p < 0.05$ , \*\* $p < 0.01$ , \*\*\* $p < 0.001$ .

studies in guinea pigs have shown that ML itself is sufficient to cause the extensive lesions, with accompanying immunosuppression by a mechanism of apoptotic cell death.<sup>7,9,20</sup> These effects have also been described in fibroblasts, macrophages, adipocytes, and muscle and are similar to our observations. The massively reduced numbers of DRG neurons and non-neuronal cells, with the remaining cells having shrunken cell bodies and bright condensed nuclei, are suggestive of apoptosis. While we have not quantified neuronal mortality in our study, examination of morphological effects showed up to 95% cell loss at the highest concentration of ML used. These findings are in keeping with the histopathological observations in necrotic lesions resulting from ML injection in guinea pig skin and from infected patients, where destruction of the subcutaneous adipose tissue leads to collapse of the epidermis and formation of a characteristic ulcer with undermined edges and nerve damage.<sup>21–23</sup> This would indicate a common mechanism by which ML targets a variety of cell types, as observed in the histopathology of tissues from infected individuals. Indeed, the potent toxicity profile of ML has prompted its development for therapeutic use as an anti-tumor agent.<sup>24,25</sup>

We observed dense clusters of PGP 9.5 positive neurons with profuse neurite outgrowth in control cultures, while ML-treated cultures showed vastly reduced numbers of neurons with shortened, faintly positive, degenerating neurites. These features are similar to those previously described with the chemotherapy drug oxaliplatin in DRG neuronal cultures, due to a toxic effect presenting as dying back of neurites.<sup>26</sup> Co-treatment with the AT<sub>2</sub>R antagonist EMA401 did not affect ML-mediated degenerative effects, indicating lack of involvement of the AT<sub>2</sub>R in ML-mediated neurotoxicity. Similarly, while Gap43 was expressed in the neurites and cell bodies of control neurons, ML-treated cultures showed a dramatic reduction in the number of surviving neurons, with Gap43 immunostaining restricted to the cell bodies of surviving neurons, accompanied by degenerating neurites. Gap43 is a marker of regenerating neurons, and its reduced expression indicates impaired regeneration and viability. The reduced expression of PGP9.5, Gap43, and  $\beta$  tubulin combined with neurite loss is consistent with reports of impaired protein synthesis after ML treatment.<sup>15</sup> These are the first such observations of ML effects in DRG neurons and are similar to reports of cell rounding and loss described in other cell types treated with ML.

Our findings in DRG cultures are in accord with reports of nerve damage underlying the hypoalgesia characteristic of Buruli ulcer in preclinical and clinical studies.<sup>10,11</sup> A clinicopathological study of 45 patients with Buruli ulcer confirmed that peripheral nerves are targeted, with severe degeneration and disruption of

nerve bundles, along with the presence of apoptotic markers.<sup>27</sup> ML toxin occurs in variable but measurable quantities in the necrotic Buruli ulcer lesions from infected patients (median 439 ng/ml)<sup>28</sup> and is found to accumulate in the peripheral blood and internal organs especially spleen of subcutaneously ML-injected mice,<sup>29</sup> indicating its ubiquitous distribution in the body. This is likely to result in altered nerve function and nerve damage, supported by the observation of degenerating neurites in our study. In accord, animal studies have shown that ML can damage nerves directly.<sup>30</sup>

In our study, confocal imaging of  $\beta$ -tubulin immunostaining combined with Mitotracker Red FM dye showed uniformly distributed speckled staining indicating individual mitochondria and  $\beta$  tubulin along the entire length of the neurites and in the cell body, in agreement with other studies.<sup>31,32</sup> ML-treated neurons on the other hand, showed near complete loss of  $\beta$  tubulin and axon degeneration, combined with clumped mitochondria accumulated in the cell body. Live cell confocal imaging with Mitotracker Green confirmed the loss of neurites and clumping of mitochondria in the cell bodies of ML-treated neurons. These observations may be related to the effect of increased mitochondrial membrane depolarization reported in keratinocyte cell lines treated with ML.<sup>4</sup> Neuronal mitochondria are normally involved in retrograde and anterograde movement, and mitochondrial clustering in the cell body is associated with impaired trafficking of mitochondria to the distal axons, due to an imbalance in transport. Bidirectional transport of mitochondria normally occurs within actively growing axons,<sup>31,32</sup> via motor proteins along microtubule tracks,<sup>32</sup> and are withdrawn from non-growing axons and areas of low metabolic demand.<sup>31</sup> Mitochondrial trafficking, as with other organelles, is subject to the phosphorylation status of microtubule-associated proteins, depending on a regulated balance between phosphatases and kinases.<sup>33,34</sup> As microtubule-dependent transport of mitochondria is a critical factor for maintaining local ATP generation in the distal processes of neurons, particularly relevant due to the extensive lengths of peripheral nerve fibers, accumulation of mitochondria in the cell body indicates disruption of these processes, potentially leading to impaired neuronal function. Mitochondrial clustering in the neuronal cell body is a characteristic feature of neurodegenerative disorders, associated with increased microtubule associated protein tau expression and its hyperphosphorylation, as seen in Alzheimer's disease.<sup>35</sup> Proteomic studies have previously shown reduction of regulators of microfilaments, microtubules, and collagen in ML-treated fibroblasts.<sup>36</sup> Thus, the loss of  $\beta$  tubulin, axon degeneration, and mitochondrial clustering following ML treatment in our study provides a morphological basis for impaired neuronal function.

As hypoalgesia is a characteristic feature of Buruli ulcer, we examined the functional effects of ML on capsaicin-mediated calcium influx via the TRPV1 receptor. The TRPV1 receptor is a  $\text{Ca}^{2+}$  permeable, non-selective cation channel that is expressed in the plasma membrane of sensory neurons and is activated by noxious signals including temperatures above  $42^\circ\text{C}$ , protons (low pH), inflammatory mediators, and plant-derived chemicals such as capsaicin, the pungent ingredient of chilli peppers, to mediate the sensation of pain via calcium influx.<sup>37</sup> One of the mechanisms regulating TRPV1 sensitivity involves cAMP-dependent PKA,<sup>38,39</sup> and the reduced expression of TRPV1 in patients with sensory neuropathy is correlated with reduced nociceptor function.<sup>40</sup> In vitro studies have shown the importance of TRPV1 activity in filopodial extension and maintenance of neurites via the enhanced expression of tubulin and myosin IIA and IIIA motors.<sup>41</sup> Our results showed that capsaicin responses in human DRG neurons were dose dependently inhibited in the presence of ML, an acute reversible effect, as capsaicin sensitivity was restored following immediate washout. Rat DRG neurons also showed dose dependent inhibition of capsaicin responses by ML at similar doses to those used in previous studies.<sup>4,12</sup> The functional effects of ML preceded the morphological effects, which were apparent only after several hours in culture. Mechanistic insight can be derived from the abolition of ML-mediated TRPV1 inhibition by the protein phosphatase 2B (calcineurin) inhibitor cyclosporine and the phosphodiesterase inhibitor IBMX: both result in increased cAMP that may rescue TRPV1 function by phosphorylation and sensitization.<sup>39,42,43</sup> It should be noted that these are acute prophylactic effects, their ability to reverse inhibition, and long-term actions deserve further investigation. Our study also suggests that rDRG neurons may be more sensitive to the effects of ML compared with human neurons, as the presence of 100 nmol/L ML resulted in more than 80% inhibition in rat neurons, while inhibition was observed in human neurons at higher concentrations (200 ng/ml), although the eventual effects were similar.

It is not clear to what extent the  $\text{AT}_2\text{R}$  is specifically targeted by ML in vivo, as the ML concentrations reported in one study to stimulate  $\text{AT}_2$  receptors were very high, in the 3  $\mu\text{g}/\text{ml}$  range (c. 4  $\mu\text{mol}/\text{L}$ ),<sup>12</sup> whereas the ML levels required to cause hyperpolarization of rat hippocampal neurons in vitro<sup>12</sup> and found in tissues after infection, were one to two orders of magnitude lower. This study also reported similar binding affinity of ML at micromolar levels to the  $\text{AT}_1\text{R}$  and  $\text{AT}_2\text{R}$ , but ML only activated  $\text{AT}_2\text{R}$ , and that ML hyperpolarization of rodent hippocampal cultured neurons was inhibited by the  $\text{AT}_2\text{R}$  antagonist PD123,319.<sup>12</sup> Our findings, and those of others, indicate diminished activity in DRG nociceptors by  $\text{AT}_2\text{R}$  antagonists across the range of

in vitro and animal pain models and clinical trials of neuropathic pain (our unpublished observations in patients with chemotherapy-induced painful neuropathy).<sup>44-48</sup> EMA401 inhibited AngII and capsaicin responses in rat- and human-cultured DRG neurons with  $\text{IC}_{50}$  of 10 nmol/L.<sup>44</sup> This contrast could reflect differences in  $\text{AT}_2\text{R}$  signaling between CNS (hippocampal) and DRG neurons. In our present study, the  $\text{AT}_2\text{R}$  agonist AngII did not affect ML-mediated inhibition of capsaicin responses in DRG neurons. As treatment of DRG neurons for 48 h with combined EMA401 and ML did not prevent cell loss or neurite degeneration, and EMA401 did not prevent acute functional effects of ML, it is unlikely that  $\text{AT}_2\text{R}$  antagonism would prevent ML-induced pathology in primary sensory neurons.

The effects of ML in different cell types may underlie the lack of inflammatory pain in Buruli ulcer. Danser and Anand,<sup>49</sup> and others, have suggested that the absence of inflammatory pain in Buruli ulcer results from ML effects on both inflammatory cells and cutaneous nociceptors. ML inhibits protein translocation into the endoplasmic reticulum resulting in the deficit of cytokines.<sup>15</sup> Such an effect would explain the lack of inflammation, secretion of inflammatory cytokines, and, thereby, the lack of inflammatory pain sensation. TRPV1 inhibition observed in the presence of ML may contribute to the hypoalgesia associated with Buruli ulcer prior to nerve damage, resembling the cutaneous hypoalgesia and loss of nociceptor terminals in *M. Leprae* infected individuals.<sup>50</sup> The studies collectively point to ML-mediated energy depletion and toxicity by a common mechanism in a variety of cell types, targeting which may provide a strategy for novel treatments.

## Conclusion

ML treatment results in profound morphological and functional effects in human and rDRG neurons, which are likely to underlie the hypoalgesia characteristic of Buruli ulcer.

## Acknowledgments

The authors wish to acknowledge the support of the National Institute for Health Research (NIHR) Biomedical Research Centre (BRC) Imaging and FACS Facility at the Hammersmith Campus (Imperial College Healthcare NHS Trust in partnership with Imperial College London). We are grateful to Professor Y. Kishi (Harvard University, USA) for generously providing the Mycolactone A/B samples for this study.

## Authors' contributions

YY, MS, MF, TQ, AM, and PA collected the clinical tissues and performed the human tissue studies. UA and YEK contributed to the in vitro experiments; TM, CB, and PA

contributed to the design and supervision of the human in vitro and tissue studies. All authors read and approved the final manuscript.

### Declaration of Conflicting Interests

CB and PA were consultants and members of the Spinifex Pharmaceuticals Scientific Advisory Board, and TM was the CEO of Spinifex Pharmaceuticals, Inc.

### Funding

The author(s) disclosed receipt of the following financial support for the research, authorship, and/or publication of this article: This study was supported by Spinifex Pharmaceuticals, Inc., which was acquired by Novartis International AG in June 2015.

### References

- WHO. Treatment of *Mycobacterium Ulcerans* Disease (Buruli Ulcer). *Guidance for Health Workers*, 2012; www.who.int/mediacentre/factsheets/fs199/en/ (accessed 1 June 2016).
- Einarsdottir T and Huygen K. Buruli ulcer. *Hum Vaccines* 2011; 7: 1198–1203.
- Walsh DS, Prttaels F and Myers WM. Buruli ulcer: advances in understanding *Mycobacterium Ulcerans* infection. *Dermatol Clin* 2011; 29: 1–8.
- Bozzo C, Tiberio R, Graziola F, et al. A *Mycobacterium ulcerans* toxin, mycolactone, induces apoptosis in primary human keratinocytes and in HaCaT cells. *Microbes Infect* 2010; 12: 1258–1263.
- Gronberg A, Zettergren L, Bergh K, et al. Antioxidants protect keratinocytes against *M. ulcerans* mycolactone cytotoxicity. *PLoS One* 2010; 5: e13839.
- Dobos KM, Small PL, Deslauriers M, et al. *Mycobacterium Ulcerans* cytotoxicity in an adipose cell model. *Infect Immun* 2001; 69: 7182–7186.
- George KM, Chatterji D, Gunawardana G, et al. Mycolactone: a polyketide toxin from *Mycobacterium Ulcerans* required for virulence. *Science* 1999; 283: 854–857.
- Snyder DS and Small PL. Uptake and cellular actions of mycolactone, a virulence determinant for *mycobacterium ulcerans*. *Microb Pathol* 2003; 34: 91–101.
- George KM, Pascopella L, Welty DM, et al. A *Mycobacterium ulcerans* toxin, mycolactone, causes apoptosis in guinea pig ulcers and tissue culture cells. *Infect Immun* 2000; 68: 877–883.
- Goto M, Nakanaga K, Aung T, et al. Nerve damage in *Mycobacterium ulcerans*-infected mice: probable cause of painlessness in Buruli ulcer. *Am J Pathol* 2006; 168: 805–811.
- En J, Goto M, Nakanaga K, et al. Mycolactone is responsible for the painlessness of *Mycobacterium Ulcerans* infection (Buruli Ulcer) in a murine study. *Infect Immun* 2008; 76: 2002–2007.
- Marion E, Song OR, Christophe T, et al. Mycobacterial toxin induces analgesia in Buruli Ulcer by targeting the angiotensin pathways. *Cell* 2014; 157: 1565–1576.
- Phillips R, Sarfo FS, Guenin-Macé L, et al. Immunosuppressive signature of cutaneous *Mycobacterium ulcerans* infection in the peripheral blood of patients with buruli ulcer disease. *J Infect Dis* 2009; 200: 1675–1684.
- Guenin-Mace L, Carrette F, Asperti-Boursin F, et al. Mycolactone impairs T cell homing by suppressing microRNA control of L-selectin expression. *Proc Natl Acad Sci USA* 2011; 108: 12833–12838.
- Hall BS, Hill K, McKenna M, et al. The pathogenic mechanism of the *Mycobacterium Ulcerans* virulence factor, mycolactone, depends on blockade of protein translocation into the ER. *PLoS Pathogens* 2014; 10: 1–14.
- Kishi Y. Chemistry of mycolactones, the causative toxins of Buruli Ulcer. *Proc Natl Acad Sci USA* 2011; 108: 6703–6708.
- Rang HP, Bevan S and Dray A. Chemical activation of nociceptive peripheral neurons. *Br Med Bull* 1991; 3: 534–548.
- Caterina MJ, Leffler A, Malmberg AB, et al. Impaired nociception and pain sensation in mice lacking the capsaicin receptor. *Science* 2000; 288: 306–313.
- Anand U, Otto WR, Sanchez-Herrera D, et al. Cannabinoid receptor CB2 localisation and agonist-mediated inhibition of capsaicin responses in human sensory neurons. *Pain* 2008; 138: 667–680.
- Read JK, Heggie CM, Meyers WM, et al. Cytotoxic activity of *Mycobacterium ulcerans*. *Infect Immun* 1974; 9: 1114–22.
- Guarner J, Bartlett J, Whitney EA, et al. Histopathologic features of *Mycobacterium ulcerans* infection. *Emerg Infect Dis* 2003; 9: 651–656.
- Hayman J and McQueen A. The pathology of *Mycobacterium ulcerans* infection. *Pathology* 1985; 17: 594–600.
- Peduzzi E, Groeper C, Schutte D, et al. Local activation of the innate immune system in Buruli ulcer lesions. *J Invest Dermatol* 2007; 127: 638–645.
- Hegggers JP, Robson MC, Yetter, et al. Tumoricidal effects of *mycobacterium ulcerans* toxin on murine adenocarcinoma (C3HBA). *J Surg Oncol* 1979; 11: 161–169.
- Lee T-Y. Anticancer agent comprising mycolactone. Patent EP 1343496 A1, 2003.
- Anand U, Otto WR and Anand P. Sensitization of capsaicin and icilin responses in oxaliplatin treated adult rat DRG neurons. *Mol Pain* 2010; 6: 82.
- Zavattaro E, Boccafoschi F, Borgogna C, et al. Apoptosis in Buruli ulcer: a clinicopathological study of 45 cases. *Histopathology* 2012; 61: 224–236.
- Sarfo FS, Phillips RO, Zhang J, et al. Kinetics of mycolactone in human subcutaneous tissue during antibiotic therapy for *Mycobacterium ulcerans* disease. *BMC Infect Dis* 2014; 14: 202.
- Hong H, Coutanceau E, Leclerc M, et al. Mycolactone diffuses from *Mycolactone ulcerans*-infected tissues and targets mononuclear cells in peripheral blood and lymphoid organs. *PLoS Negl Trop Dis* 2008; 2: e325.
- En J, Ishii N and Goto M. Role of mycolactone in the nerve damage of Buruli ulcer (*Mycobacterium ulcerans* infection). *Nihon Hansenbyo Gakkai Zasshi* 2011; 80: 5–10.

31. Morris RL and Hollenbeck PJ. The regulation of bidirectional mitochondrial transport is coordinated with axonal outgrowth. *J Cell Sci* 1993; 104: 917–927.
32. Morris RL and Hollenbeck PJ. Axonal transport of mitochondria along microtubules and F-actin in living vertebrate neurons. *J Cell Biol* 1995; 131: 1315–1326.
33. Ebnet A, Godeman R, Stamer K, et al. Overexpression of tau protein inhibits kinesin-dependent trafficking of vesicles, mitochondria and endoplasmic reticulum: implications for Alzheimer's disease. *J Cell Biol* 1998; 143: 777–794.
34. Mandell JW and Banker GA. A spatial gradient of Tau protein phosphorylation in nascent axons. *J Neurosci* 1996; 16: 5727–5740.
35. Stoothoff W, Jones PB, Spires-Jones TL, et al. Differential effect of three-repeat and four-repeat tau on mitochondrial axonal transport. *J Neurochem* 2009; 111: 417–427.
36. Gama JB, Ohlmeier S, Martins TG, et al. Proteomic analysis of the action of the Mycobacterium Ulcerans toxin mycolactone: targeting host cells cytoskeleton and collagen. *PLoS Negl Trop Dis* 2014; 8: e3066.
37. Benham CD, Davis JB and Randall AD. Vanilloid and TRP channels: a family of lipid-gated cation channels. *Neuropharmacology* 2002; 42: 873–888.
38. Bolyard LA, Van Looy JW and Vasko MR. Sensitization of rat sensory neurons by chronic exposure to forskolin or “inflammatory cocktail” does not downregulate and requires continuous exposure. *Pain* 2007; 88: 277–285.
39. Mohapatra DP and Nau C. Desensitization of capsaicin-activated currents in the vanilloid receptor TRPV1 is decreased by the cyclic AMP-dependent protein kinase pathway. *J Biol Chem* 2003; 278: 50080–50090.
40. Atherton DD, Facer P, Roberts KM, et al. Use of the novel contact heat evoked potential stimulator (CHEPS) for the assessment of small fibre neuropathy: correlations with skin flare responses and intra-epidermal nerve fibre counts. *BMC Neurol* 2007; 7: 21.
41. Goswami C and Hucho T. TRPV1-expression dependent initiation and regulation of filopodia. *J Neurochem* 2007; 103: 1319–1333.
42. Docherty RJ, Yeats JC, Bevan S, et al. Inhibition of calcineurin inhibits the desensitization of capsaicin-evoked currents in cultured dorsal root ganglion neurons from adult rats. *Pflugers Arch* 1996; 431: 828–837.
43. Bhawe G, Zhu W, Wang H, et al. cAMP-dependent protein kinase regulates desensitization of the capsaicin receptor (VR1) by direct phosphorylation. *Neuron* 2002; 35: 721–731.
44. Anand U, Facer P, Yiangou Y, et al. Angiotensin II type 2 receptor (AT<sub>2</sub>R) localization and antagonist mediated inhibition of capsaicin responses and neurite outgrowth in human and rat sensory neurons. *Eur J Pain* 2013; 17: 1012–26.
45. Smith MT, Wyse BD and Edwards SR. Small molecule angiotensin II type 2 receptor (AT<sub>2</sub>R) antagonists as novel analgesics for neuropathic pain: comparative pharmacokinetics, radioligand binding, and efficacy in rats. *Pain Med* 2013; 14: 692–705.
46. Smith MT, Lau T, Wallace VC, et al. Analgesic efficacy of small-molecule angiotensin II type 2 receptor antagonists in a rat model of antiretroviral toxic polyneuropathy. *Behav Pharmacol* 2014; 25: 137–46.
47. Muralidharan A, Wyse BD and Smith MT. Analgesic efficacy and mode of action of a selective small molecule angiotensin II type 2 receptor antagonist in a rat model of prostate cancer-induced bone pain. *Pain Med* 2014; 15: 93–110.
48. Rice AS, Dworkin RH, McCarthy TD, et al. EMA401-003 study group. EMA401, an orally administered highly selective angiotensin II type 2 receptor antagonist, as a novel treatment for postherpetic neuralgia: a randomised, double-blind, placebo controlled phase 2 clinical trial. *Lancet* 2014; 383: 1637–1647.
49. Danser AH and Anand P. The angiotensin II type 2 receptor for pain control. *Cell* 2014; 157: 1504–1506.
50. Facer P, Mathur R, Pandya SS, et al. Correlation of quantitative tests of nerve and target organ dysfunction with skin immunohistology in leprosy. *Brain* 1998; 121: 2239–47.